Concept of the equiphase sphere for light scattering by nonspherical dielectric particles

Zhigang Chen and Allen Taflove

Department of Electrical and Computer Engineering, Northwestern University, Evanston, Illinois 60208

Vadim Backman

Department of Biomedical Engineering, Northwestern University, Evanston, Illinois 60208

Received June 6, 2003; revised manuscript received August 20, 2003; accepted August 20, 2003

We introduce the concept of the equiphase sphere for light scattering by nonspherical dielectric particles. This concept facilitates the derivation of a simple analytical expression for the total scattering cross section of such particles. We tested this concept for spheroidal particles and obtained a bound on the minor-to-major axis ratio for the valid application of this technique. We show that this technique yields results that agree well with the rigorous numerical solution of Maxwell's equations obtained with the finite-difference time-domain method. The new technique has the potential to be extended to the study of light scattering by arbitrarily shaped convex dielectric particles.

OCIS codes: 290.5850, 290.0290.

1. INTRODUCTION

The physical basis and phenomenology of light scattering by small particles is of interest in a variety of science and engineering disciplines.[1,2] It is well known that light scattering by homogeneous or layered spheres comprised of isotropic dielectric materials can be analyzed with the Mie theory and its extensions.[2,3] However, because most particles of interest are neither spherical nor homogeneous, their scattering properties cannot be obtained analytically. Numerical methods for solving Maxwell's equations or approximate techniques are needed in such circumstances.

In previous work[4] we have shown numerically and analytically that the spectral dependence of the total scattering cross section of randomly inhomogeneous dielectric spheres of size in the resonant range can closely resemble that of their homogeneous counterparts with volume-averaged refractive index. The next step is to understand how departing from a spherical shape affects the total scattering cross section. For scattering by nonspherical particles, there exists no universal analogy to the Mie theory. It is not practical to develop a theory for each conceivable particle shape. But it is possible to construct a method that will include the effect of particle shape in a simplified way.

A prototypical nonspherical particle is the spheroid. Spheroids are attractive for modeling light scattering by nonspherical particles because the spheroidal shape can be changed from mildly aspherical to needle-like (prolate) or disk-like (oblate) by varying just the ratio of the major to the minor axis, i.e., the aspect ratio. Therefore the spheroidal particle becomes a natural choice when one wants to extend studies of scattering from spherical particles to nonspherical particles. The exact analytical solution for a single homogeneous, isotropic spheroid by use of the separation-of-variables method was pioneered by Asano and Yamamoto[5] and then was significantly improved by Voschinnikov and Farafonov.[6] This complex procedure involves an infinite set of linear algebraic equations for the unknown expansion coefficients that has to be truncated and solved numerically. For spheroids significantly larger than a wavelength and/or for large refractive indices, the system of linear equations becomes large and ill-conditioned. Moreover, the computation of vector spheroidal wave functions is a difficult mathematical and numerical problem. Results obtained with this approach indicate that small-diameter, highly elongated spheroids have a scattering behavior comparable to that of infinite circular cylinders with properly defined cross-section diameter.[7]

In this paper we introduce the concept of the equiphase sphere for light scattering by nonspherical dielectric particles. The equiphase sphere is defined as the sphere that gives rise to the same maximum phase shift of the penetrating light as the nonspherical particle of interest. This concept facilitates the derivation of a simple analytical expression for the total scattering cross section of nonspherical particles when $(n-1)kd \gg 1$ and $(n-1) < 1$, where k is the incident wave number, d is the characteristic size of the particle, and n is the refractive index of the particle.

To demonstrate the application of our equiphase sphere concept, we report studies of the effects of eccentricity and polarization on light scattering by a single homogeneous, isotropic dielectric spheroid that used the modified Wentzel–Kramers–Brillouin (WKB) approximation and the finite-difference time-domain (FDTD) method. Our approximate technique advances the well-known and influential anomalous diffraction theory of van de Hulst,[2] which has been a foundation of numerous advances in the light-scattering community over the past half century. Our new approximate technique is demonstrated to have

1084-7529/2004/010088-10$15.00

good agreement with the FDTD simulations in calculating the total scattering cross section, and it furthermore reveals a fundamental frequency oscillation of the total scattering cross section of a dielectric spheroid with periodicity of an equiphase sphere.

2. BASELINE PROBLEM: THE HOMOGENEOUS DIELECTRIC SPHEROID

Now we conduct an approximate analysis of how the eccentricity of a dielectric spheroid affects the wavelength dependence of its total scattering cross section. A similar procedure has been used successfully to analyze the total scattering cross section of a randomly inhomogeneous dielectric sphere.[4] The total scattering cross section of a particle much larger than the incident wavelength can be estimated with the WKB technique when $(n - 1)kd \gg 1$ and $(n - 1) < 1$,[8,9] where k is the incident wave number, d is the characteristic size of the particle, and n is the refractive index of the particle. In this approximation the electric field inside the particle is approximated by a field that propagates inside the particle with the wave number of the medium of the particle. However, this approximation neglects the scattering contribution that is due to surface effects. To improve accuracy, the total scattering cross section can be represented as the sum of two terms:

$$\sigma_s = \sigma_s^{(v)} + \sigma_s^{(s)}, \tag{1}$$

where $\sigma_s^{(v)}$ represents the contribution that is due to the volume of the scattering particle and $\sigma_s^{(s)}$ is the "edge term,"[10,11] which accounts for the contribution that is due to the sharp discontinuity of the refractive index at the particle surface. For a particle with characteristic size d and refractive index n, $\sigma_s^{(s)}$ can be approximated on the basis of the work of Nussenzveig and Wiscombe[12] as

$$\sigma_s^{(s)} \approx 2S_m(kd/2)^{-2/3}[1 + \chi(kd, n)], \tag{2}$$

where S_m is the maximal geometrical cross section of the particle and χ describes the interference of the surface waves, which gives rise to the high-frequency ripple structure in the wavelength dependence of the total scattering cross section. We will neglect χ in the following discussions because the ripple structure is typically averaged out in most realistic measurements owing to the size distribution of the scattering particles. For an ellipsoid with axes of length a, b, and c, we have

$$\sigma_s^{(s)} \approx 2S_m[k(abc)^{1/3}/2]^{-2/3}, \tag{3}$$

$$\sigma_s^{(v)} = 2\,\mathrm{Re}\left(\int\int_S \{1 - \exp[i\xi(\mathbf{r})]\}\mathrm{d}^2\mathbf{r}\right), \tag{4}$$

where S is the maximum geometrical cross section of the particle in the plane transverse to the direction of propagation of the incident light, $\mathbf{r}$ is a vector in the plane that S lies in, and $\xi(\mathbf{r})$ is the relative phase shift of a light ray that passes through the particle along a straight trajectory with respect to the phase shift of a light ray propagating outside the particle. The relative phase shift $\xi(\mathbf{r})$ can be written as

$$\xi(\mathbf{r}) = \int_{L(\mathbf{r})} k[n(\mathbf{r}) - 1]\mathrm{d}l, \tag{5}$$

where the integration is performed over the path L of the light ray inside the particle.

Now we consider a prolate spheroid $(a > b = c)$ with a major axis of length a and minor axes of length b. Referring to Fig. 1, we define three electromagnetic wave modes for different combinations of plane-wave incidence and polarization with respect to the major axis of the spheroid: (a) TM mode (the magnetic field vector **H** perpendicular to the major axis and the electric field vector **E** parallel to the major axis), (b) TE mode (**E** perpendicular to the major axis and **H** parallel to the major axis), and (c) TEM mode (both **E** and **H** perpendicular to the major axis). For the TE and TM modes, the path L of the light ray inside the particle is

$$L \approx b\{1 - \epsilon^2[|\mathbf{r}|/R(\mathbf{r})]^2\}^{1/2}\cos[\gamma'(\mathbf{r}) - \gamma(\mathbf{r}) + \phi(\mathbf{r})], \tag{6}$$

where the eccentricity factor $\epsilon^2 = 1 - [b/R(\mathbf{r})]^2$, $R(\mathbf{r})$ is the radius of the particle measured in plane S along direction $\mathbf{r}$ (such that $b \leqslant 2R \leqslant a$), and γ and γ' are the angles of incidence and refraction, respectively, at the particle surface. γ, γ', and ϕ satisfy $\tan\gamma = (|\mathbf{r}|b/a^2)\{1 - [|\mathbf{r}|/R(\mathbf{r})]^2\}^{-1/2}$, $\sin\gamma' = \sin\gamma/n$, and $\tan\phi = (|\mathbf{r}|/b)\{1 - [|\mathbf{r}|/R(\mathbf{r})]^2\}^{-1/2}$. As a result, $\xi(\mathbf{r})$ can be expressed as

$$\xi(\mathbf{r}) \approx kb(n - 1)\{1 - 1/n^2 + [|\mathbf{r}|/R(\mathbf{r})]^2/n^2\}^{1/2}[1 + \delta L(\mathbf{r})], \tag{7}$$

where

$$\delta L = [L(\mathbf{r}) - b\,\eta(\mathbf{r})]/[b\,\eta(\mathbf{r})],$$

$$\eta(\mathbf{r}) = \{1 - 1/n^2 + [|\mathbf{r}|/R(\mathbf{r})]^2/n^2\}^{1/2}.$$

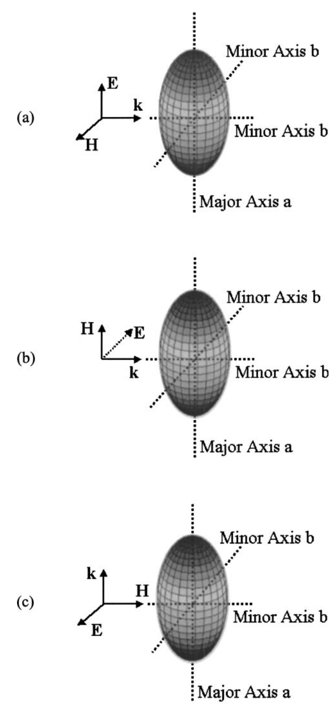

Fig. 1. Schematic of different combinations of incidence and polarization state of light. (a) TM mode, (b) TE mode, (c) TEM mode.

If $kb(n - 1)\delta L < \pi/2$, we can expand the integrand in Eq. (4) to perform the integration analytically. This yields

$$\sigma_s = \sigma_s^{(s)} + 2S[1 - 2n \sin\rho/\rho + 4n \sin^2(\rho/2)/\rho^2], \tag{8}$$

where $\rho = kb(n - 1)$ is the maximum phase shift of a light ray propagating through the spheroid along a straight path. Thus, by substituting relation (3) into Eq. (8), we obtain for the TE and TM modes

$$\sigma_s = (\pi ab/2)[k(ab^2)^{1/3}/2]^{-2/3} + (\pi ab/2)[1 - 2n \sin\rho/\rho + 4n \sin^2(\rho/2)/\rho^2]. \tag{9}$$

Similarly, for the TEM mode, we obtain

$$\sigma_s = (\pi ab/2)[k(ab^2)^{1/3}/2]^{-2/3} + (\pi b^2/2)[1 - 2n \sin\rho_a/\rho_a + 4n \sin^2(\rho_a/2)/\rho_a^2], \tag{10}$$

where $\rho_a = ka(n - 1)$. Equations (9) and (10) can be combined into one general equation:

$$\sigma_s = \sigma_s^{(v)} + \sigma_s^{(s)} = (\pi ab/2)[k(ab^2)^{1/3}/2]^{-2/3} + 2S[1 - 2n \sin\rho/\rho + 4n \sin^2(\rho/2)/\rho^2]. \tag{11}$$

Here, for the TM and TE modes, $2S = \pi ab/2$ and $\rho = kb(n - 1)$; and for the TEM mode, $2S = \pi b^2/2$ and $\rho = ka(n - 1)$.

3. CONCEPT OF THE EQUIPHASE SPHERE

In Eq. (11), ρ represents the maximum phase lag of a light ray propagating through the spheroid along a straight path. For the three electromagnetic wave modes defined above, the total scattering cross section exhibits an oscillatory behavior as a function of wavelength. The periodicity of this oscillatory behavior is determined by the maximum phase shift ρ and is thus proportional to the maximum path length of a light ray propagating inside the spheroid, which equals b for the TE and TM modes or a for the TEM mode. The ρ-dependent terms in Eq. (11), which determine the periodicity of the oscillatory behavior of the total scattering cross section, are similar to those in the equation obtained by van de Hulst for a homogeneous spherical particle with low refractive index[13]:

$$\sigma_s = 2S[1 - 2 \sin\rho/\rho + 4 \sin^2(\rho/2)/\rho^2]. \tag{12}$$

Here $S = \pi(d/2)^2$ and $\rho = kd(n - 1)$, where d is the diameter of the spherical particle; ρ represents the maximum phase lag of a light ray propagating through the spherical particle along a straight path. Thus, by comparing Eq. (11) with Eq. (12), we are able to define the equiphase sphere as the sphere that gives rise to the same maximum phase shift of the penetrating light as the spheroid or the nonspherical particles of interest. For the homogeneous spheroid that we discuss, the corresponding equiphase sphere has the same refractive index as the spheroid and has a diameter d equal to the length of the spheroid's minor axis b (for the TE and TM modes) or equal to the length of the spheroid's major axis a (for the TEM mode). The amplitude of the oscillations depends on S. If $a = b$ (i.e., the particle is spherical), Eq. (11) matches the analogous expression for a spherical particle.[4] When $n \to 1$ and $a = b$, Eq. (11) matches Eq. (12).

The oscillatory behavior of the total scattering cross section of a spheroid follows that of its equiphase sphere *in phase* provided that $(n - 1)kd \gg 1$, $(n - 1) < 1$, and $\rho\delta L(\mathbf{r}) < \pi/2$, where $\delta L(\mathbf{r})$ accounts for the deviation of $L(\mathbf{r})$ from its counterpart inside the corresponding equiphase sphere. For the TE and TM modes, $\rho\delta L(\mathbf{r}) < \pi/2$ is equivalent to

$$\begin{aligned}\beta &\equiv 4(n - 1)b\,\delta L/\lambda \\ &\approx (16/\pi^2)(b/\lambda) \\ &\quad \times [(n - 1)^2/n](1 - b/a)(1 + a^2/b^2)^{-1} < 1.\end{aligned} \tag{13}$$

For the TEM mode, $\rho\delta L(\mathbf{r}) < \pi/2$ is equivalent to

$$\begin{aligned}\beta &\equiv 4(n - 1)a\,\delta L/\lambda \\ &\approx (16/\pi^2)(a/\lambda) \\ &\quad \times [(n - 1)^2/n](1 - a/b)(1 + b^2/a^2)^{-1} < 1,\end{aligned} \tag{14}$$

where λ is the wavelength of the incident wave. Along with $(n - 1)kd \gg 1$ and $(n - 1) < 1$, relations (13) and (14) define the regime of validity of Eq. (11) for the TE and TM modes and the TEM mode, respectively. As expected, $\beta = 0$ if $a = b$ or $n = 1$. $\delta L(\mathbf{r})$ quantifies the effect of light refraction inside a spheroid compared with that inside a sphere. δL becomes smaller as the interior light propagates in a direction closer to that of the incident light. Thus δL decreases as the spheroid's refractive index or curvature decreases. For the TE and TM modes, the curvature of a spheroid appears to be smaller than that of its corresponding equiphase sphere. Here, as shown in Fig. 2(a) for $n = 1.5$ and $\lambda = 500$ nm, β increases as b/a increases, reaches a maximum at $b/a = 0.7$, and then decreases to zero at $b/a = 1$, which corresponds to a sphere. From Fig. 2(a) we see that $\beta < 1$ for all $b < a$, which means that Eq. (11) is valid for any eccentricity, and the total scattering cross-section oscillatory pattern of a spheroid follows that of its corresponding equiphase sphere in phase provided that $(n - 1)kd \gg 1$ and $(n - 1) < 1$. On the other hand, for the TEM mode, the curvature of a spheroid appears to be larger than that of its corresponding equiphase sphere. The larger curvature results in a higher δL. In this case, as shown in Figs. 2(b) and 2(c) for $n = 1.5$ and $\lambda = 500$ nm, β increases monotonically as b/a decreases from 1 to 0. When β approaches unity, the periodicity of the total scattering cross-section oscillatory pattern is altered, and the total scattering cross section of an equiphase sphere provides a poor approximation to that of a spheroid. Therefore for the TEM mode the total scattering cross section is analogous to that of its corresponding equiphase sphere only within a limited range of eccentricities. We note from relation (14) that the range of validity of this ap-

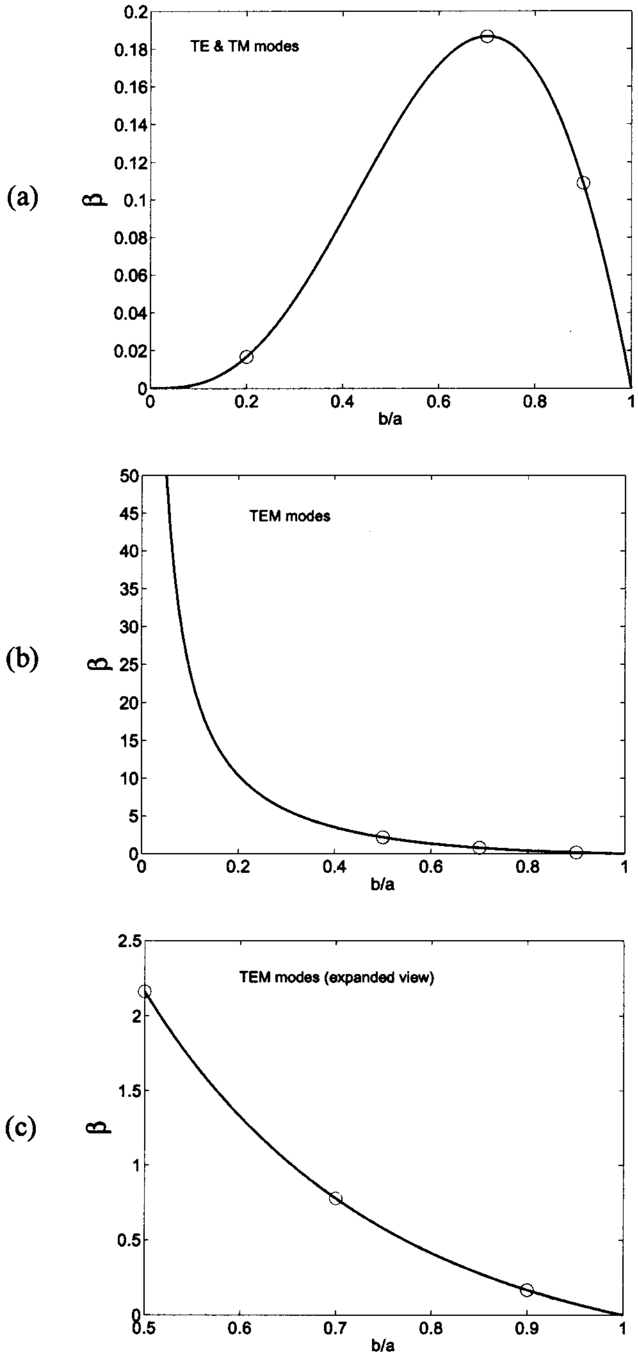

Fig. 2. Condition parameter β versus b/a ratios of spheroids for $\lambda = 500$ nm. (a) TE and TM modes, (b) TEM modes, (c) expanded view of Fig. 2(b).

proximation is substantially larger for smaller refractive index. For example, for $n = 1.1$, β does not approach 1 for b/a ratios as small as 0.2. This has important implications for modeling light scattering by biological tissues.

4. NUMERICAL RESULTS

To verify our approximate analytical results discussed above, we conducted FDTD[14] simulations to compute light scattering of a dielectric spheroid with a wide range of b/a ratios. First we verified our FDTD code by computing the scattering pattern of a homogeneous sphere and comparing the results to the Mie theory. A Gaussian pulse wave source was imposed on the simulation grid, and the scattered-field frequency response was extracted through a discrete Fourier transform run concurrently with the FDTD time stepping.[14] The perfectly-matched-layer absorbing boundary condition[15] was used in our simulations to terminate the computational lattice. A dielectric prolate spheroid of refractive index $n = 1.5$ was constructed within an FDTD space lattice that had a uniform cubic cell size of 25 nm. The prolate spheroid was generated by rotating an ellipse about its major axis of length $a = 5$ μm, thereby yielding equal minor axes of length b. Variable b/a ratios were obtained by varying b while keeping a fixed.

A. Effects of Eccentricity and Polarization

First we studied the effects of eccentricity and polarization on light scattering by a homogeneous dielectric spheroid and identified the concept of an equiphase sphere for modeling light scattering by a spheroid. Four eccentricity cases, $b/a = 0.9$, 0.5, 0.2 and 0.1 were studied. For the first case, we studied all three plane-wave modes defined in Section 2. For the other three cases, we studied only the TE and TM modes. For each case we calculated the total scattering cross section for an incident wavelength range of 500–1000 nm.

Figure 3 graphs the FDTD-calculated spheroid total scattering cross section (in units of m^2) versus wavelength for the eccentricity $b/a = 0.9$ ($a = 5$ μm, $b = 4.5$ μm). Figure 3(a) shows the results of the FDTD simulations for the TE mode (solid dots) and the TM mode (open circles). For comparison, the solid curve shows the corresponding Mie data for the corresponding equiphase sphere of the same refractive index $n = 1.5$ and a diameter equal to the length of the spheroid's minor axis, which gives rise to the same maximum phase shift of the penetrating light as the spheroid. From Fig. 3(a) we see that the spheroid's total scattering cross sections for the two modes are nearly the same. Further, the spheroid's total scattering cross section as a function of wavelength has an oscillatory pattern closely resembling that of the corresponding equiphase sphere in phase. The primary difference is that the magnitude of the spheroid's total scattering cross section is shifted upward by an approximately constant factor. This factor approximately corresponds to the difference between the spheroid's geometrical cross section transverse to the direction of wave propagation and the geometrical cross section of the equiphase sphere. Another difference is that the FDTD-calculated spheroid total scattering cross section lacks the high-frequency ripple structure of the sphere. On the basis of our previous numerical experiments,[4] we believe that this difference arises from the staircasing of the spheroid's surface within the FDTD grid, which reduces the surface-wave effects required for the appearance of the ripple structure.

Figure 3(b) repeats the study of Fig. 3(a) for the TEM mode. For this case, the phase-equivalent homogeneous sphere has a diameter equal to the length of the spheroid's major axis, 5 μm. From Fig. 3(b) we can see that

(a)

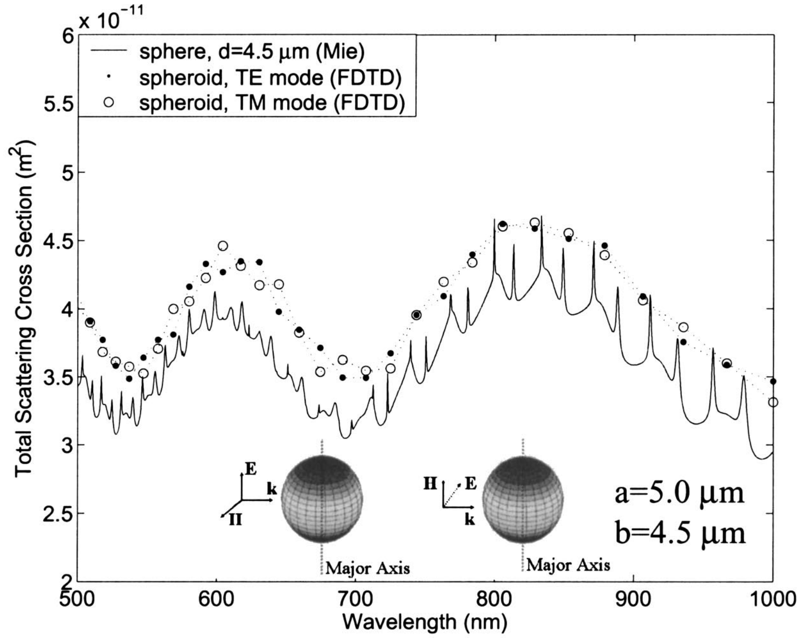

(b)

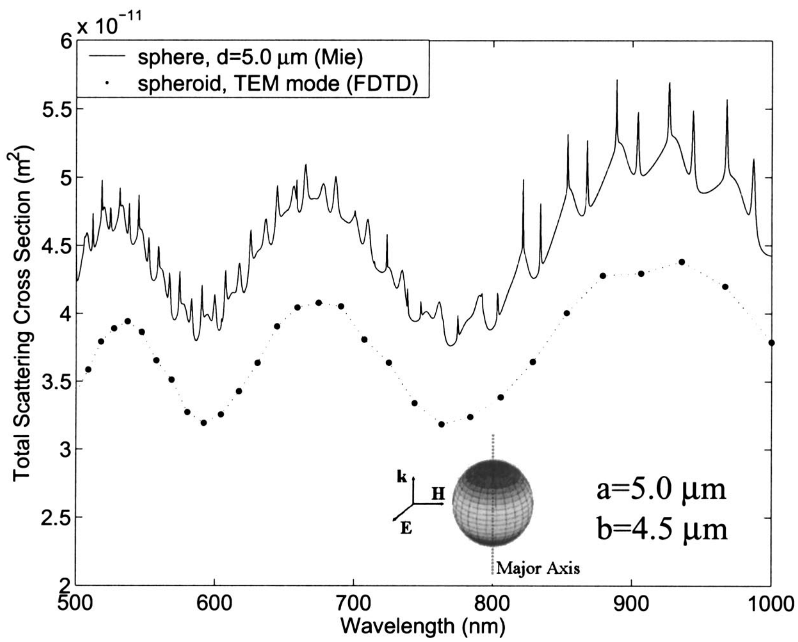

Fig. 3. (a) Total scattering cross section of ($a = 5$ μm, $b = 4.5$ μm) spheroid versus wavelength. The FDTD results for the spheroid are represented by solid dots (TE mode) and open circles (TM mode) and the Mie results for the corresponding equiphase sphere by a solid curve. (b) Corresponding results for the TEM mode.

the total scattering cross section of the spheroid as a function of wavelength has an oscillatory pattern closely resembling that of its phase-equivalent Mie counterpart in phase. We can see also that the magnitude of the total scattering cross section is shifted downward by an approximately constant factor that approximately corresponds to the difference between the spheroid's geometrical cross section transverse to the direction of wave propagation and the geometrical cross section of the equiphase sphere.

Figure 4 compares the FDTD-calculated and the Eq. (11)-calculated spheroid total scattering cross sections for the TE and TM modes for $b/a = 0.9$ ($a = 5$ μm, $b = 4.5$ μm) and $b/a = 0.5$ ($a = 5$ μm, $b = 2.5$ μm). We can see that the Eq. (11)-calculated total scattering cross section is quite close to the FDTD-calculated total scattering cross section. Moreover, the FDTD-calculated total scattering cross section illustrates that the total scattering cross section of the TE mode is similar to that of the TM mode.

Figure 5 compares the FDTD-calculated and the Eq. (11)-calculated spheroid total scattering cross section for the TE and TM modes for $b/a = 0.2$ ($a = 5$ μm, $b = 1$ μm) and $b/a = 0.1$ ($a = 5$ μm, $b = 0.5$ μm). Here we see that the Eq. (11)-calculated total scattering cross section predicts the trend of the FDTD-calculated total scattering cross section, although it begins to deviate from FDTD-calculated values. This deviation is expected since the WKB condition $[(n - 1)kd \gg 1$ and $(n - 1) < 1]$ is hardly satisfied in these two cases. For both cases the FDTD-calculated total scattering cross section of the TE mode is still similar to that of the TM mode, while their magnitudes differ slightly.

B. Range of Validity of the Approximation

Next we investigated the validity range of our analytical approximation. The validity range of the approximation is described by relation (13) for the TE and TM modes and by relation (14) for the TEM mode. The condition parameter β, which must be less than unity to ensure validity of the approximation, is plotted in Fig. 2 as a function of the b/a ratios of spheroids for $\lambda = 500$ nm. For the TE and TM modes, we studied three b/a ratios (0.2, 0.7, and 0.9), designated by circles in Fig. 2(a). We have shown in Subsection 4.A that the total scattering cross section of the TE mode is similar to that of the TM mode. Therefore here we show only the total scattering cross section of the TM mode. For the TEM mode, we studied three b/a ratios (0.5, 0.7, and 0.9), designated by circles in Figs. 2(b) and 2(c). In each case we calculated the total scattering cross section for an incident wavelength range of 500–1000 nm.

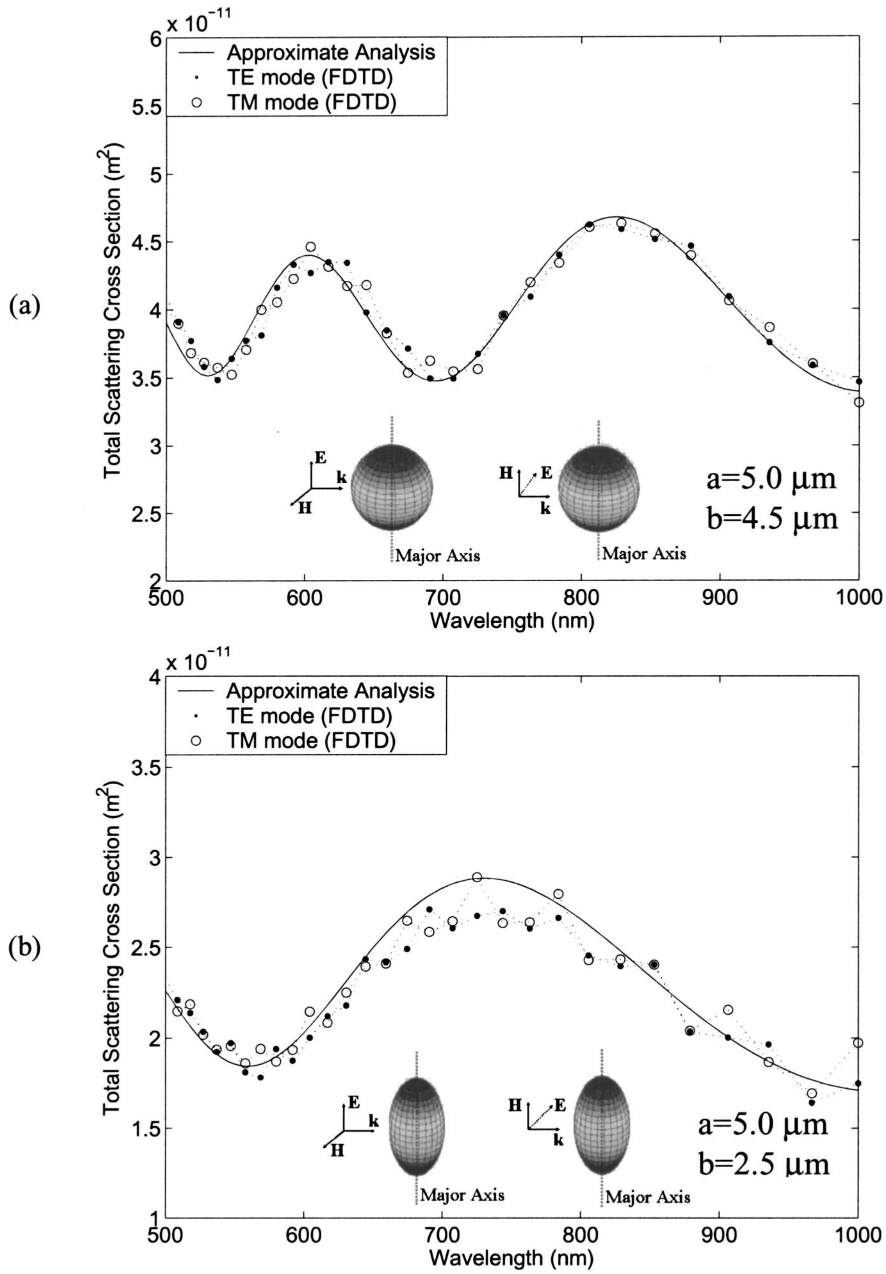

Fig. 4. (a) Total scattering cross section of ($a = 5$ μm, $b = 4.5$ μm) spheroid versus wavelength for TE and TM modes. The FDTD results are represented by solid dots (TE mode) and open circles (TM mode) and the results of the approximate analysis by a solid curve. (b) Corresponding results for ($a = 5$ μm, $b = 2.5$ μm) spheroid.

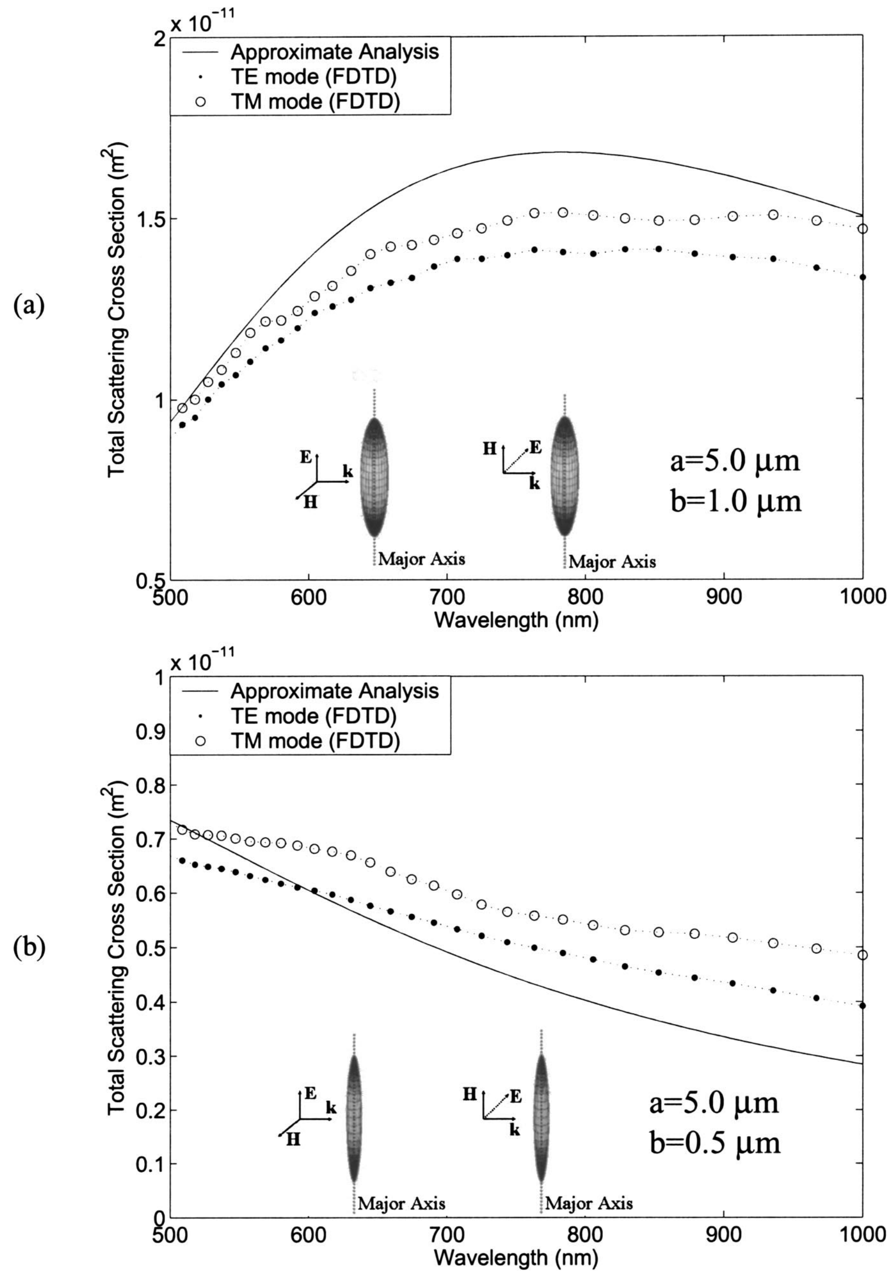

Fig. 5. (a) Total scattering cross section of ($a = 5\ \mu$m, $b = 1\ \mu$m) spheroid versus wavelength for TE and TM modes. The FDTD results are represented by solid dots (TE mode) and open circles (TM mode) and the results of the approximate analysis by a solid curve. (b) Corresponding results for ($a = 5\ \mu$m, $b = 0.5\ \mu$m) spheroid.

Figure 6 graphs the FDTD-calculated and the Eq. (11)-calculated spheroid total scattering cross sections for the TM mode versus wavelength for $b/a = 0.2$, 0.7 and 0.9, corresponding to the three b/a ratios designated by circles in Fig. 2(a). For comparison, the solid curve shows the corresponding Mie data for corresponding equiphase spheres of the same refractive index $n = 1.5$ and a diameter equal to the length of the spheroid's minor axis, which gives rise to the same maximum phase shift of the penetrating light as the spheroid. From Fig. 6 we see that the Eq. (11)-calculated total scattering cross section is quite close to the FDTD-calculated total scattering cross section. Further, both the FDTD-calculated and the Eq. (11)-calculated total scattering cross sections as a function of wavelength have oscillatory patterns closely resembling those of the corresponding equiphase spheres in phase. The primary difference is that the magnitude of the spheroid's total scattering cross section is shifted upward by an approximately constant factor. This factor approximately corresponds to the difference between the spheroid's geometrical cross section transverse to the direction of wave propagation and the geometrical cross section of the equiphase sphere. In this case (TM mode), β is well below 1 for any b/a ratios, as shown in Fig. 2(a), so it is expected that the Eq. (11)-calculated total scattering cross section will have good agreement with the FDTD-calculated total scattering cross section.

Figure 7 graphs the FDTD-calculated and Eq. (11)-calculated spheroid total scattering cross sections for the TEM mode versus wavelength for $b/a = 0.5$, 0.7, and 0.9,

(a)

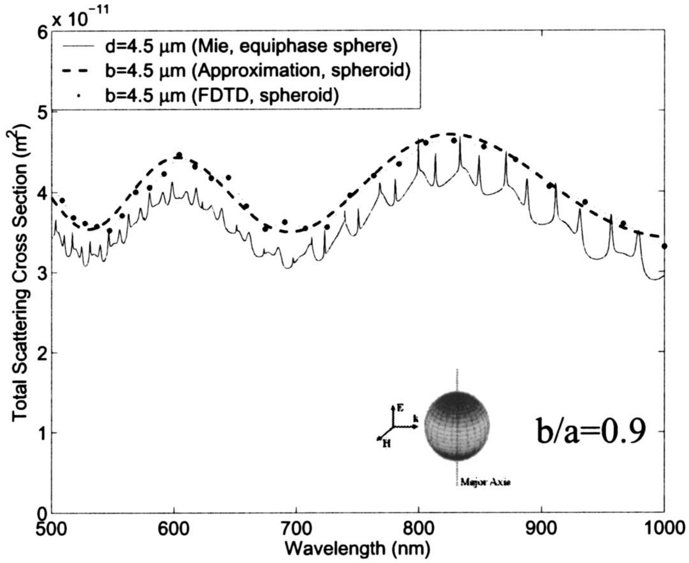

(b)

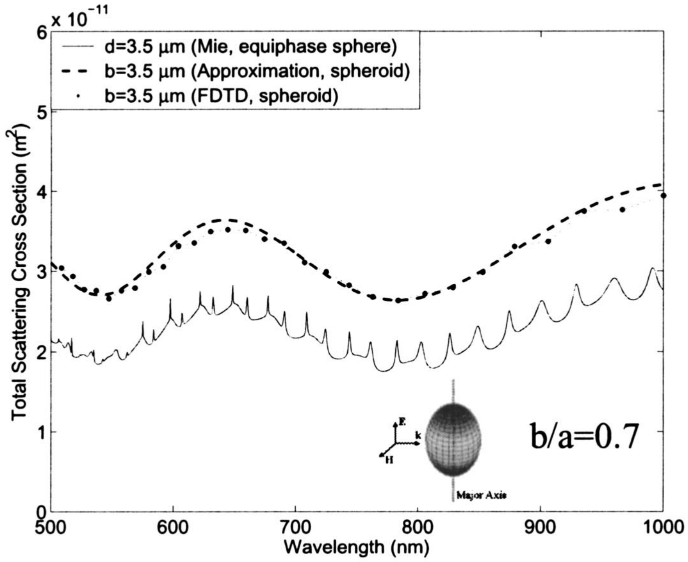

(c)

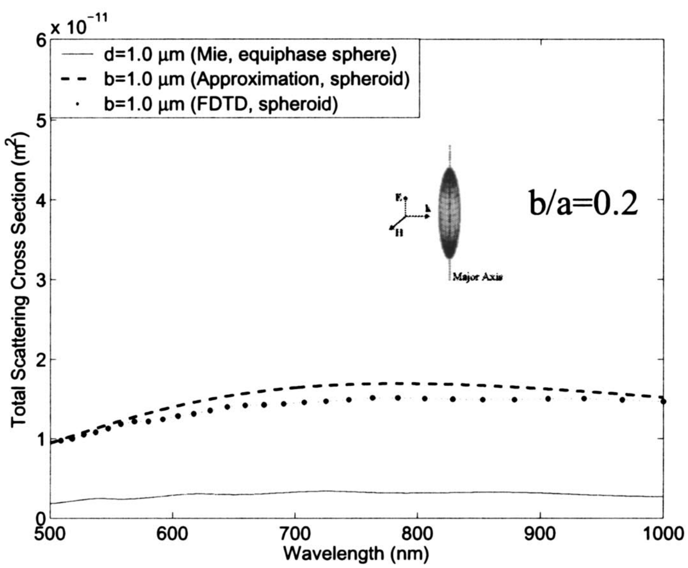

Fig. 6. Total scattering cross section of spheroids for the TM mode versus wavelength for $b/a = 0.2$, 0.7, and 0.9, corresponding to the three b/a ratios designated by circles in Fig. 2(a). (a) $b/a = 0.9$, (b) $b/a = 0.7$, (c) $b/a = 0.2$.

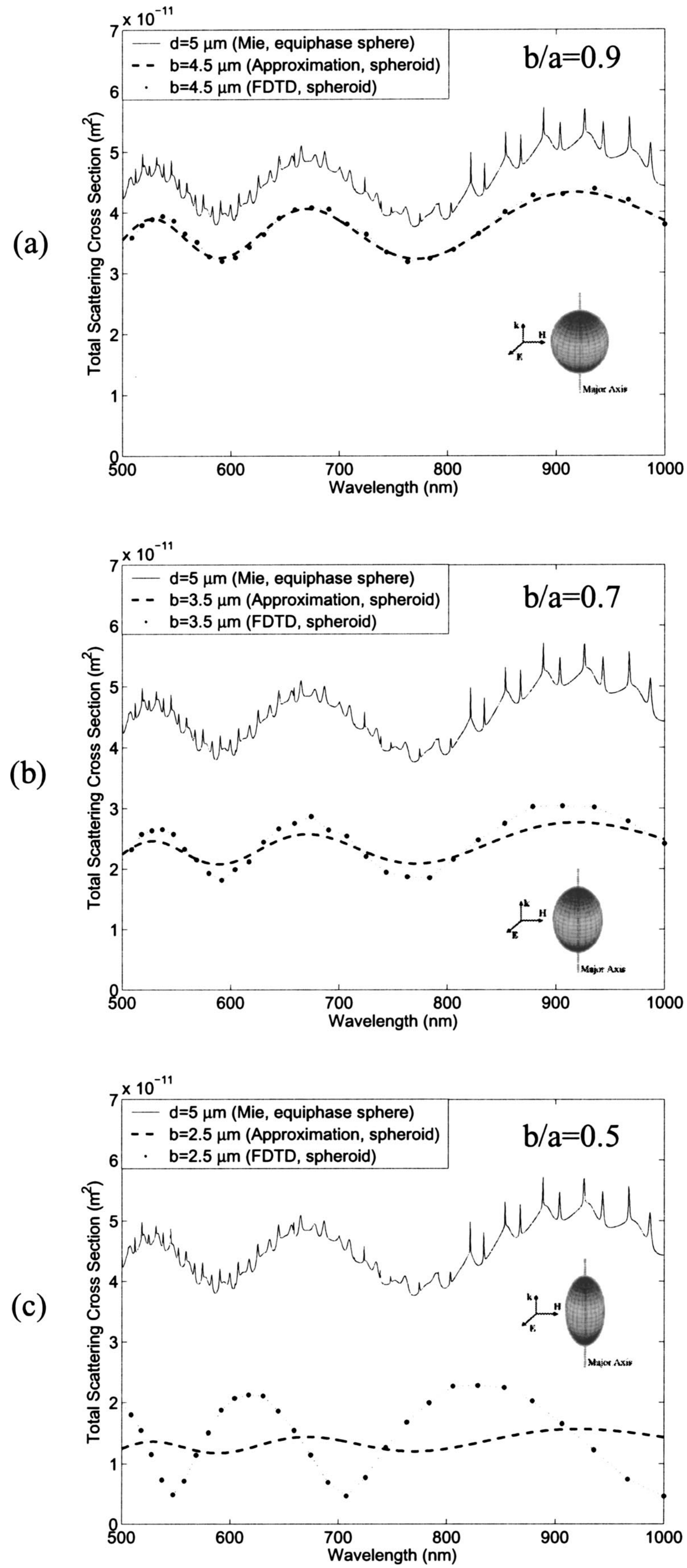

Fig. 7. Total scattering cross section of spheroids for the TEM mode versus wavelength for $b/a = 0.5$, 0.7, and 0.9, corresponding to the three b/a ratios designated by circles in Figs. 2(b) and 2(c). (a) $b/a = 0.9$, (b) $b/a = 0.7$, (c) $b/a = 0.5$.

corresponding to the three b/a ratios designated by the open circles in Figs. 2(b) and 2(c). For comparison, the solid curve shows the corresponding Mie data for corresponding equiphase spheres of the same refractive index $n = 1.5$ and a diameter equal to the length of the spheroid's major axis, which gives rise to the same maximum phase shift of the penetrating light as the spheroid. From Fig. 7 we see that the Eq. (11)-calculated total scattering cross section is quite close to the FDTD-calculated total scattering cross section for $b/a = 0.9$; it deviates slightly from the FDTD-calculated total scattering cross section for $b/a = 0.7$ and deviates significantly from the FDTD-calculated total scattering cross section for $b/a = 0.5$. This is in accordance with the behavior of β as a function of b/a. As shown in Figs. 2(b) and 2(c), β is far less than 1 for $b/a = 0.9$, close to but still less than 1 for $b/a = 0.7$, and far greater than 1 for $b/a = 0.5$. For $\beta > 1$ the validity condition for Eq. (11) is no longer satisfied, and hence we cannot use Eq. (11) to calculate the total scattering cross section of a spheroid for the TEM mode. Nevertheless, for $\beta < 1$ the Eq. (11)-calculated results for total scattering cross section as a function of wavelength have good agreement with the results for FDTD-calculated total scattering cross section and have oscillatory patterns closely resembling those of the corresponding equiphase spheres in phase.

5. SUMMARY AND CONCLUSIONS

In this paper we have identified the concept of the equiphase sphere for modeling the total scattering cross section of homogeneous, isotropic nonspherical dielectric particles. This concept leads to a simple analytical expression for the total scattering cross section of such particles that agrees well with FDTD simulations when applied to spheroids.

The single-scattering characteristic examined in this paper, the total scattering cross section of a particle, is one of the most widely used observables in light scattering transport and light scattering by random media. It plays a fundamental role in the theory of light propagation and diffusion in inhomogeneous media such as biological tissues and the turbulent atmosphere. We have focused on spheroids, which are attractive for modeling light scattering by nonspherical particles because the spheroidal shape can be changed from mildly aspherical to needle-like (prolate) or disk-like (oblate) by varying just the ratio of the major to the minor axis, i.e., the aspect ratio. Our approach provides a more accurate alternative to the present nearly ubiquitous use of the Mie theory in the regime where it loses validity. Our approach may also be used by researchers to check the validity of their use of the Mie theory to model light scattering by nonspherical particles.

Although we have limited our test cases to spheroidal particles, our approximation technique is extendable without further difficulty to the study of light scattering by an ellipsoidal particle. It can also be extended to calculate the differential scattering cross section of nonspherical particles in a manner similar to the van de Hulst approximation. In our future work we shall apply this technique to the study of light scattering by arbitrarily shaped convex particles. Our final goal is to permit relatively simple modeling of light scattering by arbitrarily shaped convex particles. This would find broad applications, including optical diagnostics of pathologies in living tissues.[16]

ACKNOWLEDGMENT

This work was supported in part by National Science Foundation grant BES-0238903.

Corresponding author Z. Chen may be reached by e-mail at z-chen@northwestern.edu.

REFERENCES

1. M. I. Mishchenko, J. W. Hovenier, and L. D. Travis, *Light Scattering by Nonspherical Particles: Theory, Measurements and Applications* (Academic, San Diego, Calif., 2000).
2. H. C. van de Hulst, *Light Scattering by Small Particles* (Dover, New York, 1981).
3. M. Kerker, *The Scattering of Light and Other Electromagnetic Radiation* (Academic, New York, 1969).
4. Z. Chen, A. Taflove, and V. Backman, "Equivalent volume-averaged light scattering behavior of randomly inhomogeneous dielectric spheres in the resonant range," Opt. Lett. **28**, 765–767 (2003).
5. S. Asano and G. Yamamoto, "Light scattering by a spheroidal particle," Appl. Opt. **14**, 29–49 (1975).
6. N. V. Voshchinnikov and V. G. Farafonov, "Optical properties of spheroidal particles," Astrophys. Space Sci. **204**, 19–86 (1993).
7. N. V. Voshchinnikov and V. G. Farafonov, "Light scattering by an elongated particle: spheroid versus infinite cylinder," Meas. Sci. Technol. **13**, 249–255 (2002).
8. A. Ishimaru, *Wave Propagation and Scattering in Random Media* (Academic, New York, 1978).
9. J. D. Klett and R. A. Sutherland, "Approximate methods for modeling the scattering properties of non-spherical particles: evaluation of the Wentzel–Kramers–Brillouin method," Appl. Opt. **31**, 373–386 (1992).
10. S. A. Ackerman and G. L. Stephens, "The absorption of solar radiation by cloud droplets: an application of anomalous diffraction theory," J. Atmos. Sci. **44**, 1574–1588 (1987).
11. A. A. Kokhanovsy and A. Macke, "Integral light scattering and absorption characteristics of large nonspherical particles," Appl. Opt. **36**, 8785–8790 (1997).
12. H. Nussenzveig and W. Wiscombe, "Efficiency factors in Mie scattering," Phys. Rev. Lett. **45**, 1490–1494 (1980).
13. H. C. van de Hulst, *Light Scattering by Small Particles* (Dover, New York, 1981), p. 176.
14. A. Taflove and S. Hagness, *Computational Electrodynamics: The Finite-Difference Time-Domain Method* (Artech, Boston, Mass., 2000).
15. J.-P. Berenger, "A perfectly matched layer for the absorption of electromagnetic waves," J. Comput. Phys. **114**, 185–200 (1994).
16. V. Backman, L. T. Perelman, J. T. Arendt, R. Gurjar, M. G. Muller, Q. Zhang, G. Zonios, E. Kline, T. McGillican, T. Valdez, J. Van Dam, M. Wallace, K. Badizadegan, J. M. Crawford, M. Fitzmaurice, S. Kabani, H. S. Levin, M. Seiler, R. R. Dasari, I. Itzkan, and M. S. Feld, "Detection of preinvasive cancer cells *in situ*," Nature **406**, 35–36 (2000).